RSC Advances

PAPER

View Article Online
View Journal | View Issue

Cite this: *RSC Adv.*, 2020, **10**, 39241

Sodium alginate/collagen composite multiscale porous scaffolds containing poly(ε-caprolactone) microspheres fabricated based on additive manufacturing technology†

Shuifeng Liu,‡[a] Da Huang,‡[b] Yang Hu,*[a] Jiancheng Zhang,[a] Bairui Chen,[a] Hongwu Zhang,[b] Xianming Dong,[a] Rongbiao Tong,[c] Yiheng Li[d] and Wuyi Zhou*[a]

Biocompatible porous scaffolds with adjustable pore structures, appropriate mechanical properties and drug loading properties are important components of bone tissue engineering. In this work, biocompatible sodium alginate (SA)/collagen (Col) multiscale porous scaffolds containing poly(ε-caprolactone) microspheres (Ms-PCL) have been facilely fabricated based on 3D extrusion printing of the pre-crosslinked composite hydrogels. The prepared composite hydrogels can be 3D extrusion printed into porous scaffolds with different designed shapes and adjustable pore structures. The hydroxyapatite (HAP) nanoparticles have been added into the SA/Col hydrogels to achieve stress dispersion and form double crosslinking networks. SA-Ca^{2+} crosslinking networks and Col–genipin (GP) crosslinking networks have been constructed to improve the mechanical properties of the scaffolds (about 2557 kPa of compressive stress at 70% strain), and reduce the swelling rate and degradation rate of SA/Col scaffolds. Moreover, the SA/Col hydrogels contain hydrophobic antibacterial drug enrofloxacin loaded Ms-PCL, and *in vitro* drug release research shows a sustained-release function of porous scaffolds, indicating the potential application of SA/Col porous scaffolds as drug carriers. In addition, the antibacterial experiments show that the composite scaffolds display a distinguished and long-term antibacterial activity against *Escherichia coli* and *Staphylococcus aureus*. Furthermore, mouse bone mesenchymal stem cells (mBMSCs) are seeded on the SA/Col composite scaffolds, and an *in vitro* biocompatibility experiment shows that the mBMSCs can adhere well on the composite scaffolds, which indicate that the fabricated composite scaffolds are biocompatible. In short, all of the above results suggest that the biocompatible SA/Col composite porous scaffolds have enormous application and potential in bone tissue engineering.

Received 23rd May 2020
Accepted 20th October 2020

DOI: 10.1039/d0ra04581k

rsc.li/rsc-advances

Introduction

Tissue engineering methods include the use of cell-seeded scaffolds to repair and replace damaged tissues, which are expected to be used to repair cartilage defects.[1–4] In order to support the specific differentiation of bone mesenchymal stem cells (BMSCs), it is very important to design scaffolds with proper structures, mechanical properties and drug loading abilities.[5–7] Among various biocompatible materials, collagen is an ideal candidate material for the preparation of cartilage tissue engineering scaffolds,[8–10] because it is a component of natural cartilage. Porous collagen scaffolds are usually prepared by firstly pouring collagen hydrogel precursors (which can be mixed with cells or therapeutic drugs) into glass tubes, and then freeze-drying to remove water and form pore structures in the collagen scaffolds.[11,12] However, the application of pure collagen scaffolds is limited by their poor mechanical properties and fast degradation speed. Low mechanical strength is not conducive to bearing compression and pull from external forces, and a fast degradation rate goes against cell differentiation and cartilage repair.[13–18] Moreover, the hydrophilic collagen scaffolds have difficulty loading hydrophobic drugs uniformly, which limits the application of collagen scaffold

[a]*Biomass 3D Printing Materials Research Center, College of Materials and Energy, South China Agricultural University, Guangzhou 510642, China. E-mail: zhouwuyi@scau.edu.cn; huyang0303@scau.edu.cn*

[b]*Department of Anatomy, Guangdong Provincial Key Laboratory of Construction and Detection in Tissue Engineering, Southern Medical University, 1023# Shatai South Road, Guangzhou 510515, China*

[c]*Department of Chemistry, The Hong Kong University of Science and Technology, Clear Water Bay, Kowloon, Hong Kong, China*

[d]*Guangzhou Trauer Biotechnology Co., Ltd., 4F, A Building, U-Best Industrial Park, No. 17 Xiangshan Road, Science Town, Guangzhou, China, 510663*

† Electronic supplementary information (ESI) available. See DOI: 10.1039/d0ra04581k

‡ Both authors contributed equally to this work.

materials in drug loading and sustained release.[19,20] In addition, currently most of the prepared collagen scaffolds consist of single-pore structures, which do not satisfy the pore requirements for the multi-scale porous structures of cartilage.[21,22]

For improving the mechanical properties of collagen scaffolds, adding suitable crosslinking agent, inlaying rigid particles and introducing double crosslinking network into collagen hydrogels are promising effective methods. Lots of chemical crosslinking agents have been used in collagen modification. Because the glutaraldehyde has excellent grafting efficiency and low cost, it is often used as the crosslinker for the collagen scaffolds, but its toxicity to human body is too strong to hinder its application.[23–26] Genipin (GP) is a natural product extracted from gardenia fruit and it is an effective collagen crosslinker. It has excellent biocompatibility and some health care effects, such as anti-inflammatory and liver protection.[27–29] Therefore, GP is chosen as the suitable crosslinking agent of collagen,[30–32] and it is expected that GP can play a key role in crosslinking of collagen. Moreover, the introduction of rigid particles into hydrogels can also improve the mechanical properties of hydrogels. Rigid particles such as gold and silver nanoparticles were introduced into collagen to enhance the strength and stability of hydrogels.[33–35] However, the nanoparticles modified collagen hydrogels did not result in significant cartilage regeneration, probably because the type of rigid particles conducive to cartilage regeneration awaited to be explored. In this work, rigid hydroxyapatite (HAP) nanoparticles with good biocompatibility and outstanding osteogenic ability were added to collagen hydrogel matrix to enhance the mechanical properties.[36–38] As for double crosslinking network, sodium alginate (SA) as a natural polymer material, was chosen to construct the double crosslinking network because of its good biocompatibility, non-toxicity, biodegradability and nontoxic degradation products.[39,40] SA would chelate with calcium released from HAP nanoparticles to form SA/HAP crosslinking network to a certain extent. Then, the SA/HAP crosslinked network and Col/GP crosslinked network made up the double crosslinking network together.

At present, most of the scaffolds prepared by gas foaming technology[41,42] or emulsion template method[43–45] have a single pore structure, which is inconsistent with the multi-scale pore structure of cartilage. The natural cartilage contains a multi-scale pore structure, including micro-pores and macro-pores coexist. 3D printing, a rapid prototyping technology, has received increasing attention on the preparation of biological scaffolds materials.[46,47] Based on discretization and stacking principles, 3D printing technology has the ability to construct a complete pore structure. The shape, pore size and connectivity of the porous scaffold can be precisely adjusted by 3D printing technology.[48–50] Thus 3D printing method is a promising preparation approach to obtain bionic cartilage scaffolds.[51,52] In this way, macro-pore structure could be obtained through 3D printing, and the micro-pore structure could be acquired by freeze-drying of hydrogel scaffolds.

Herein, we have developed a composite Col/SA gel scaffolds with multiscale pore structures and containing hydrophobic drug-loaded polycaprolactone microspheres (Ms-PCL), which are prepared basing on extrusion 3D printing. Fig. 1 is the schematic illustration of fabrication of SA/Col composite multiscale porous scaffolds containing Ms-PCL. To be specific, HAP nanoparticles were served as a particulate emulsifier to stabilize Pickering emulsion incorporating PCL and hydrophobic drug enrofloxacin (ENR) in the oil phase. The Ms-PCL were obtained after solvent evaporation of Pickering emulsion. Then, the Ms-PCL were added into a homogeneous slurry containing HAP nanoparticles, collagen and SA. However, it was found that the viscosity of the above slurry was too low to be used for 3D printing. In order to solve this problem, D-gluconic acid δ-lactone (GDL) was added into the above slurry, which could assist in the Ca^{2+} release from HAp nanoparticles, and in turn form SA-Ca^{2+} crosslinking network to obtain printable pre-crosslinked hydrogel of high viscosity. Moreover, the above pre-crosslinked hydrogel was used as ink and 3D-printed into the porous hydrogel scaffolds. Furthermore, the biocompatible SA/Col multiscale porous scaffolds containing Ms-PCL were formed after freeze drying. The morphology, mechanical properties, degradability, drug release behaviour, antimicrobial property and biocompatibility of porous scaffolds were discussed in detail.

Experimental

Materials

SA, Col, GDL and ENR were purchased from Aladdin Reagent Co. (Shanghai, China). HAP nanoparticles were supported by Beijing Deke Daojin Company (Beijing, China), and were approximately stick-like nanoparticles with the short-axis lengths ranging from 15 to 50 nm and the long-axis lengths ranging from 70 to 230 nm (see Fig. S1†). PCL (MW = 80 000 g mol^{-1}) was offered by Shandong Medical Instrument Research Institute (Jinan, China). Dichloromethane (CH_2Cl_2) were purchased from Tianjinshi Baishi Chemical Co., Ltd (Tianjin, China). GP was bought from Zhixin Biotechnology Co., Ltd (Jiangxi, China) and Mouse bone mesenchymal stem cells (mBMSCs) were purchased from the American Type Culture Collection (ATCC, Manassas, VA).

Preparation of PCL microspheres

Firstly, 0.06 g ENR and 0.225 g PCL were added respectively into 3 mL of CH_2Cl_2 and then stirred for 30 min to obtain the oil phase. Secondly, 0.3 g HAP nanoparticles were added into 9 mL of H_2O and sonicated for 30 min to get the water phase. Thirdly, the oil phase was added in batches into the water phase and immediately emulsified with a vortex mixer at 3000 rpm after every addition to form oil-in-water (O/W) emulsion. Different concentrations of HAP nanoparticles (3%, 5%, 7%) were used to fabricate O/W emulsion. Finally, CH_2Cl_2 from emulsion droplets was evaporated at room temperature to obtain PCL microspheres.

Fabrication of the biocompatible porous scaffolds

The porous scaffolds containing PCL microspheres were fabricated basing on 3D extrusion printing of the pre-crosslinked SA/Col hydrogel ink. First, 0.6 g HAP nanoparticles, 0.1 g GP and 0.3 g Col were added into 30 mL H_2O, and then stirred about 30 min at 37 °C to form the even slurry. Second, 1.2 g SA was put in the above even slurry and then stirred for another 2 h to acquire the SA/HAP/

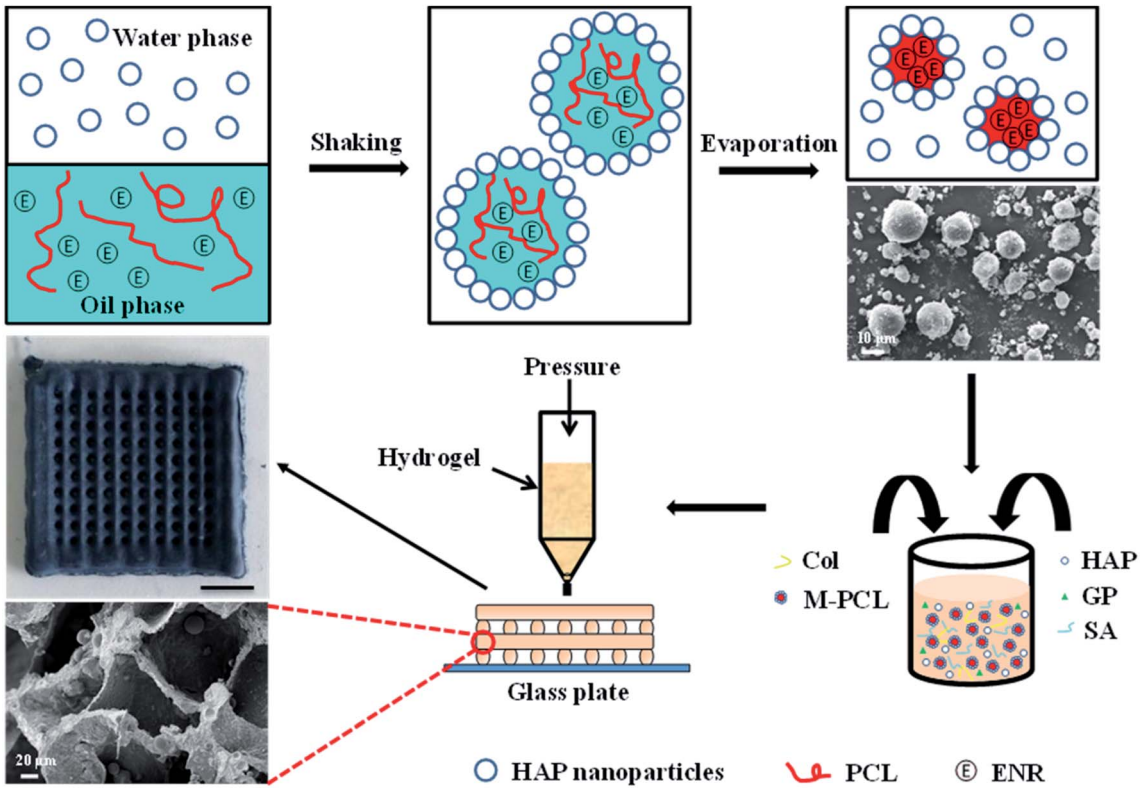

Fig. 1 Schematic illustration of the fabrication of SA/Col composite multiscale porous scaffolds containing Ms-PCL fabricated based on 3D printing technology.

Col suspension. Third, 0.3 g GDL and 0.3 g PCL microspheres were put into the above suspension to form the pre-crosslinked SA/HAP/Col hydrogel. At last, the porous scaffolds containing PCL microspheres were prepared based on our previous research[53] and the related experimental steps were are as follows. A designed 20 × 20 × 5 mm^3 scaffold was formed through an ADT-TV5300DJ three axis dispensing control system. Afterwards, the above pre-crosslinked SA/HAP/Col hydrogels were injected into a polypropylene syringe equipping with a 0.84 mm screw dispensing needle. Then, the polypropylene syringe filled with the SA/HAP/Col pre-crosslinked hydrogels was connected to the dispensing system to obtain the designed structure. At last, the biocompatible porous scaffolds were soaked in 10 wt% $CaCl_2$ solution in order to further cross-linking and then took out to freeze drying.

Characterization

The prepared W/O emulsions were observed with an optical microscope (Carl Zeiss, German), and the size distribution of the emulsions were measured with the image analysis software (Nano Measurer 1.2 software). Fourier transform infrared (FTIR) spectra of samples were recorded by a Thermo Fisher infrared spectrometer (Nicolet iS10, USA). The interior structures of the scaffolds were observed through a Zeiss EVO 18 scanning electron microscope (SEM) at 10 kV. Transmission electron microscopy (TEM) test of HAP nanoparticles were carried out on FEI transmission electron microscope (Tecnai G220, USA). The mechanical properties of porous scaffolds were assessed by the Shenzhen SANS universal testing machine (UTM-4204, China).

Rheology

The rheological properties of hydrogel precursors were measured by an MCR502 rheometer (Anton Parr, Austria) equipped with stainless steel parallel plate geometry (25 mm diameter) at 25 °C. The viscosity test was performed at the shear rate ranging from 0.1 s^{-1} to 100 s^{-1}. All measurements were carried out three times, and the average was calculated.

Swelling test

In order to research the swelling characteristics of porous scaffolds, different samples were weighed and immersed in deionized water and phosphate buffer solution (PBS, pH 7.4) at 37 °C for a period of time. Afterwards, the samples were took out from the solution and dried superficially with a filter paper and weighed again. The weight of the swollen scaffolds (W_{S1} g) was recorded at different time period and compared with the dry weight (W_{S0} g) of the related scaffolds. The swelling rate (S) was obtained from the following equation:

$$S = [(W_{S1} - W_{S0})/W_{S0}] \times 100\%$$

Degradation behavior

Degradation rate of porous scaffolds were studied by immersing samples (0.5 cm × 0.5 cm × 0.2 cm, $n = 3$) in 10 mL PBS solution (pH = 7.4) at 37 °C during different time intervals (1, 3, 6, 9, 12, 15, 18, 21 days). Before immersing in PBS, the weight of samples

was measured and noted as W_0 g. Then, samples were removed from PBS and washed in distilled water to remove buffer salts. At last, the samples were put into the freeze-drying machine for freeze-drying 24 h and then weighed (W_1 g). The degradation rate (D) was calculated using the following equation:

$$D = [(W_0 - W_1)/W_0] \times 100\%$$

In vitro drug release

The *in vitro* ENR release research was probed in PBS solution (pH 7.4) with the shaking speed of 100 rpm at 37 °C. The ENR release behaviors of ENR-loaded porous scaffolds were measured using an UV2300 UV-vis spectrophotometer at 274 nm. In detail, approximately 15 mg of ENR-loaded porous scaffolds were immersed into 50 mL of PBS (pH = 7.4) solution. At prescribed time intervals, about 2 mL of the released medium was taken to measurement and then poured the above solution back in the container, and kept shaking. Furthermore, the cumulative release rate of ENR was calculated basing on the calibration absorbance–concentration curve established from standard PBS solutions of ENR. Each sample was measured in more than three times and an average value was obtained. In this research, the porous scaffolds were fabricated with different ENR-loaded contents in PCL microspheres (0.2 wt%, 0.8 wt%, 1.4 wt%).

Antibacterial activity

The antibacterial activities of porous scaffolds against *Staphylococcus aureus* (*S. aureus*) and *Escherichia coli* (*E. coli*) were evaluated *via* the inhibition zone method.[54,55] First, the bacterial suspensions were dispersed in the aseptic broth medium, and the bacterial concentration was about 10^7 CFU mL^{-1}. Second, 0.6 mL of the inoculation bacterial suspensions were spread on the nutrient agar plates uniformly. Third, the porous scaffold samples with the size of 1 mm in height and 6 mm in diameter were put on the surface of the nutrient agar plates. The antibacterial activities of the porous scaffold samples could be observed through the nutrient agar plates after incubating at 37 °C for a period of time. The clear inhibition zones appeared on the nutrient agar plates around the testing scaffold samples indicated that the relevant scaffold samples possessed the antibacterial activity. Moreover, the related porous scaffolds without ENR were selected as the control samples. Every experiment was repeated for three times.

In vitro cytocompatibility assessment

To evaluate the *in vitro* cytocompatibility assessment of porous scaffolds, mBMSCs were seeded on the porous scaffold samples. In detail, all of the porous scaffolds samples were put into 24-well tissue culture plates and sterilized with an electron beam sterilizer at the dose of 25 KGy for 2 h. After soaking in cell culture fluid for 12 h, mBMSCs suspension was seeded onto the porous scaffolds samples at a density of 3000 cells per cm^2. After cultured in a cell incubator with 5% CO_2 at 37 °C for a period of time, cells on every samples were washed with phosphate buffered saline (PBS) three times and then treated with ethidium homodimer-1 (0.5 μM) and calcein AM (0.25 μM) (Live/Dead viability kit, Molecular Probes) for 45 min. Cells were observed under an inverted fluorescent microscope (IX53, Olympus).

The proliferation rate of mBMSCs was calculated with AlamarBlue assay (Molecular Probes) after cultured for 1, 3 and 5 days, respectively. Briefly, the porous scaffolds samples were sterilized for 2 h and put into the 24-well tissue culture plates as previous mention. The mBMSCs were seeded on the samples at a density of 3000 cells per cm^2, and the culture medium was refreshed every two days. At every time point of assay, the mBMSCs were incubated in the culture medium containing 10% (v/v) AlamarBlue reagent in 5% CO_2 for 4 h at 37 °C, then 100 μL solution from each example was removed into a 24-well tissue culture plates and read at 530/600 nm in a SpectraMax fluorescence microplate reader (Molecular Devices).

Results and discussion

Preparation of PCL microspheres and pre-crosslinked composite hydrogels

In this study, PCL microspheres were fabricated through solvent evaporation of O/W emulsion templates stabilized by approximately stick-like HAP nanoparticles. Thereinto, CH_2Cl_2 solution containing ENR and PCL was served as the oil phase, and aqueous solution containing HAP nanoparticles was used as the water phase. The prepared O/W emulsions were observed with a Carl Zeiss optical microscope, and the optical images of the O/W emulsions are presented in Fig. 2a–c. The optical images had shown a clear tendency that the increase of HAP contents resulted in the decrease in emulsion droplet size. The emulsion droplet size distribution was further analysed by measuring 120 droplets from the optical images using the Nano Measurer 1.2 software, and the results are presented in Fig. 2d–f. As seen, the calculated droplet sizes for all the O/W emulsions were mainly distributed in the range of 10–20 μm, and this ratio decreased with the increase of HAP contents, which was also observed for the presence of droplets diameters <8 μm. In turn, the number of large droplets in the range of 18–24 μm decreased as the content of HAP nanoparticles increased in the O/W emulsions. This phenomenon should be attributed to the reason that increasing the HAP nanoparticle concentration resulted in more nanoparticles to act as stable particles, which could stabilize a larger interfacial area and make denser nanoparticle layer on the oil–water interface, in turn reduced the average size of the emulsion droplets. Herein, 3 wt% HAP content was selected to prepare PCL microspheres by solvent evaporation of O/W emulsion droplets. The prepared microspheres were ball-shaped microspheres (see Fig. S2a†), and contained C, O, P and Ca elements (see Fig. S2b†), which indicated the existence of HAP in the microspheres. Furthermore, FTIR analysis results of pure PCL microspheres, ENR and ENR-loaded PCL microspheres are presented in Fig. S2c.† In the spectrum of PCL microspheres, the strong peaks at 1724 cm^{-1} and 1041 cm^{-1} were ascribed to the stretching vibration of C=O and C–O bonds, respectively. In the spectrum of ENR, the peaks at 1738 cm^{-1} and 1256 cm^{-1} were attributed to the

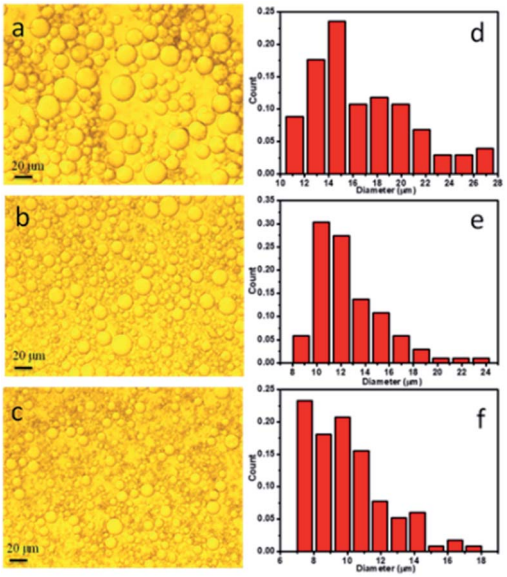

Fig. 2 Optical micrographs of the O/W emulsions fabricated with different HAP contents of (a) 3 wt%, (b) 5 wt% and (c) 7 wt%; size distribution graphs of the O/W emulsions with different HAP contents of (d) 3 wt%, (e) 5 wt% and (f) 7 wt%.

stretching vibration of C=O and C–O in –COOH, and 1630 cm^{-1} was assigned to the carbonyl stretching vibration in pyridine ketone. Besides, 1509 cm^{-1} and 1471 cm^{-1} were ascribed to the frame vibration of benzene ring. In contrast with the spectrum of PCL microspheres, the spectrum of ENR-loaded PCL microspheres appeared new peaks at 1738 cm^{-1}, 1630 cm^{-1}, 1509 cm^{-1}, 1471 cm^{-1} and 1256 cm^{-1}, which referred to the characteristic absorption peaks of ENR. These above results indicated that the drug ENR had been loaded in the PCL microspheres successfully.

The quantitative examination of the viscosity of the pre-crosslinked composite hydrogels was carried out using an MCR-502 rheometer at 25 °C. The viscosity curves of the composite hydrogels samples after pre-crosslinking for 24 h are shown in Fig. 3. With an increase in the shear rate, it was obvious that the viscosities of all pre-crosslinked composite hydrogels significantly decreased. The result showed that the prepared composite hydrogels were pseudoplastic gels and had shear thinning behaviour, which allowed for a reduction of the hydrogels viscosity by about 1 orders of magnitude when the shear rate was varied from 0.1 s^{-1} to 100 s^{-1}. The shear thinning behavior helped the pre-crosslinked hydrogels to flow out from the printing nozzle during the extrusion printing process, and then obtained viscous products to maintain the printing shape. In contrast, the pre-crosslinked hydrogels without Ms-PCL and GP had a lower viscosity of 199 000 mPa s at the low shear rate (0.1 s^{-1}). The addition of Ms-PCL and GP can increase the viscosity of the pre-crosslinked hydrogels to 248 000 mPa s. That was because the crosslinking reaction between GP and collagen led to the increase compactness of the hydrogel networks. These results indicated that the addition of Ms-PCL and GP increased the viscosity of composite hydrogels, thus

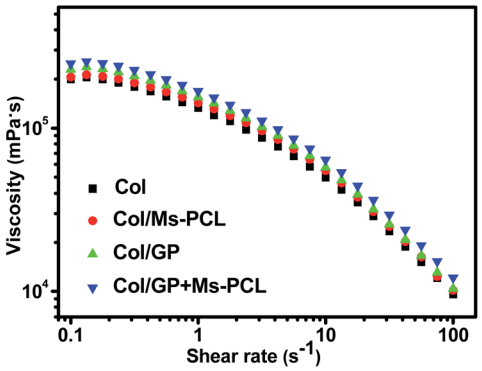

Fig. 3 Curves of viscosity as a function of shear rate for composite hydrogels prepared with different formulations.

helping to maintain the shape of 3D printing. Fig. S3† shows the porous scaffolds fabricated by 3D extrusion printing with composite hydrogels as bio-ink. It can be seen from the photographs that the printing scaffolds have a clear network structure and can well maintain the printing shapes.

Fabrication of the biocompatible porous scaffolds

Fig. 4 displays the SEM images of porous scaffolds prepared with different Ms-PCL concentrations. As shown in the SEM images of porous scaffolds without Ms-PCL (Fig. 4a), clear and regular pore structure could be seen; while in the porous scaffolds with Ms-PCL added, there were many spheres attaching to the wall of the holes or embedding in the scaffolds. With the increase of Ms-PCL contents, the number of regular spherical Ms-PCL in the scaffold increased correspondingly. Moreover, Fig. 5 is the SEM images of porous scaffolds before and after crosslinking with GP. The porous scaffolds without being crosslinked by GP showed interconnected pores with the size about 100 μm, while the GP-crosslinked porous scaffolds displayed a more lamellar porous structure. Overall, the GP-crosslinked scaffold network became dense and could bear more physics pressure, thus assisting in improving the mechanical properties of the scaffolds. The multistage microporous structure helps to improve the stress dispersion ability of the scaffolds and their stability in the solution. In addition, the different size pores of porous scaffolds have different biomedical functions, such as: small size pores are conducive to cell adhesion and growth, and large scale pore size ensures effective material exchange and transfer ability in the environment.

Mechanical properties of porous scaffolds

Mechanical properties are also critical for the implanted tissue engineering scaffolds, because they will withstand complex physiological loads after implantation. However, the pure Col porous scaffolds have poor mechanical properties. To research the mechanical properties of the porous scaffolds, the compression tests were conducted. Fig. 6a and b display the related compressive stress–strain curves of the porous scaffold samples. It was observed that the Ms-PCL contents and GP had

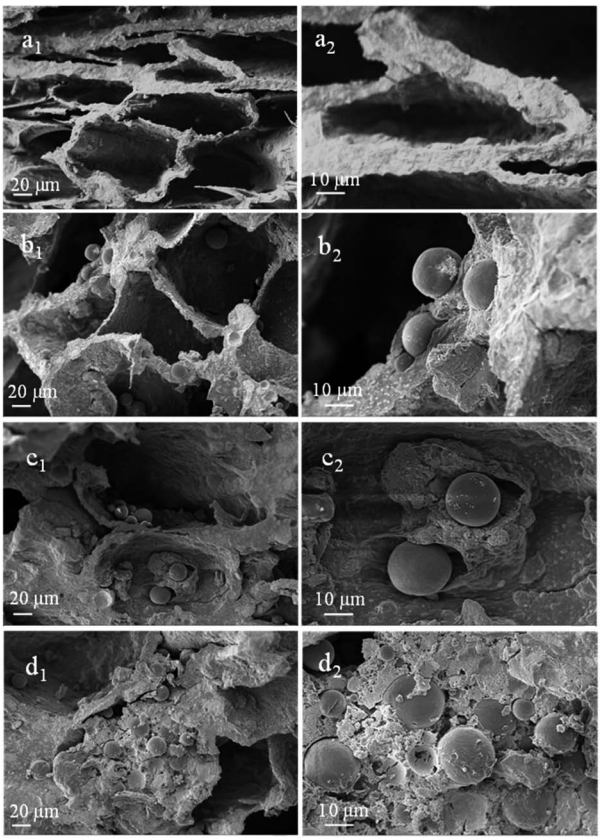

Fig. 4 SEM images of porous scaffolds with different Ms-PCL concentrations: (a_1 and a_2) 0 wt%, (b_1 and b_2) 3 wt%, (c_1 and c_2) 5 wt% and (d_1 and d_2) 7 wt%.

an influence on the compression properties of porous scaffolds. The relevant average compressive stress values of porous scaffolds with different Ms-PCL contents of 0, 3, 5, and 7 wt% at 70% strain were 304, 343, 468 and 649 kPa, respectively. The above results indicated that the compressive stresses at 70% strain increased gradually with Ms-PCL contents. The main

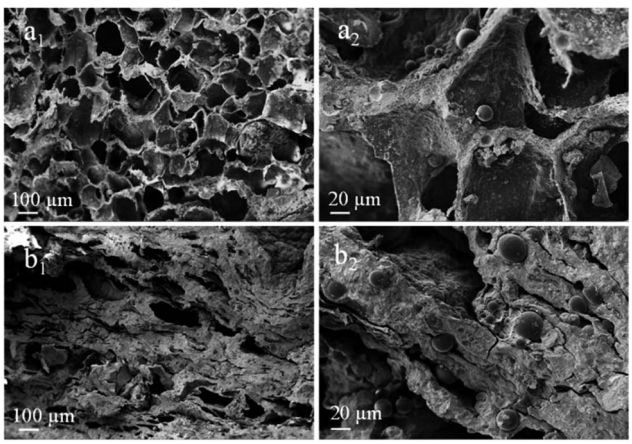

Fig. 5 SEM images of porous scaffolds with Ms-PCL concentrations at 5 wt% before and after crosslinking with GP: (a_1 and a_2) before crosslinking, (b_1 and b_2) after crosslinking.

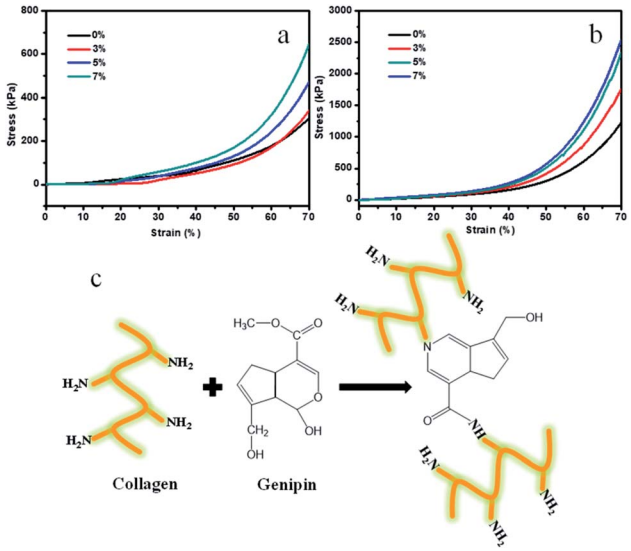

Fig. 6 The compression stress–strain curves of porous scaffolds: (a) porous scaffolds with different Ms-PCL contents; (b) porous scaffolds with different Ms-PCL at the same GP content, and (c) a diagram of the crosslinking mechanism of Col and GP.

reason was that with the increase of Ms-PCL contents from 0 to 7 wt%, more rigid particles could act as stress points in the pore walls of porous scaffolds which could improve stress transfer from the polymer matrix to the Ms-PCL particles.

Furthermore, the addition of GP as a crosslinking agent played an important role in reinforcing the polymer matrix. After adding GP, a double crosslinking network structure was formed in the SA/Col composite hydrogels system. The average compressive stress values of porous scaffolds with different Ms-PCL contents (0, 3, 5, and 7 wt%) after adding GP at 70% strain were 1219, 1760, 2350 and 2557 kPa, respectively. Obviously, with the addition of GP, the compressive stress of the materials can be increased to 4 to 5 times under the same compressive strain at 70% and increased to about 13 times compared with pure Col porous scaffolds (see Fig. S4†). That was because after adding GP, it had chemical crosslinking reaction with Col, which was beneficial to improve the mechanical properties of Col hydrogel materials. Based on the knowledge of GP crosslinking,[56–59] a possible reaction mechanism between Col and GP are shown in Fig. 6c. In the reaction pathway, the nucleophilic amino groups of Col attack the olefinic carbon atom at C-3 in GP, followed by opening of the dihydropyran ring and the nucleophilic substitution of the ester group in GP to connect the Col molecules. Therefore, adding GP as the crosslinking agent can greatly enhance the mechanical properties of Col scaffold materials.

In vitro swelling and degradation properties

Fig. 7a and b show the time-dependent curves of the swelling rate for the porous scaffolds immersed in deionized water and PBS. As seen, porous scaffolds rapidly absorbed a large amount of water in the swelling solution. The swelling rate of porous scaffolds changed rapidly in the first two hours and approached

to the swelling equilibrium in eight hours. Moreover, the swelling rate of porous scaffolds in PBS solution was greater than that in water. This was because when the porous scaffold were immersed in PBS solution, some Ca^{2+} in the scaffolds were exchanged with Na^{+} in PBS solution, resulting in the replacement of partial calcium alginate to sodium alginate. This result caused that the gel network of the samples became loose, which could absorb more moisture and get higher swelling rate. In addition, the swelling rate of scaffolds can be greatly reduced by adding GP. This is because the crosslinking reaction between GP and Col enhanced the crosslinking density of the scaffold network, and the scaffold network became denser, so the corresponding swelling rate of porous scaffolds decreased. Furthermore, with the addition of PCL microspheres, the swelling rate of porous scaffolds decreased to some extent. The main reason was that the water absorption of the scaffolds was mainly attributed to the gel network, and the water absorbability of the microspheres was limited. When the microspheres were added, the ratio of the gel network to the composite porous scaffolds was reduced, so the swelling rate of the composite porous scaffolds was decreased.

Fig. 7c presents the results for *in vitro* degradation rate of porous scaffolds measurements. It is obvious that GP-free porous scaffolds samples had the maximum degradation rate at 60.4% in 21 days, while the samples with the adding of GP had a degradation rate of 35.9% at the same degradation time. The results indicated that the degradation rate of porous scaffolds could be effectively reduced by adding GP. Because the chemical crosslinking between GP and Col increased the crosslinking degree of SA/Col hydrogels, thereby reducing the degradation rate of SA/Col hydrogels materials.

Moreover, after 3 days of degradation, the Col/Ms-PCL sample lost about 35.6% of its initial weight, which was 23% higher than that Col/GP + Ms-PCL sample. The most probable reason was that the Ms-PCL had been effectively immobilized in GP and Col crosslinked hydrogel networks, thereby eliminating their leakage from the gel network.

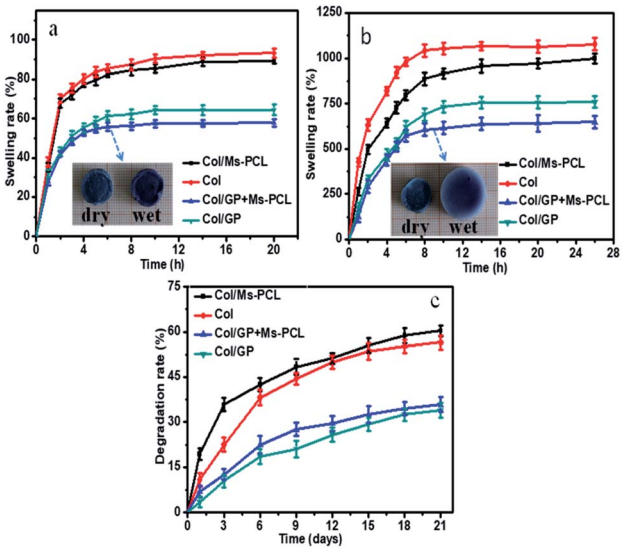

Fig. 7 Swelling rate of porous scaffolds after immersion in H_2O (a) and PBS (b) as a function of time, and (c) degradation rate of porous scaffolds during 21 days.

In vitro drug delivery characterization

The release behaviour of ENR *in vitro* from the ENR-loaded scaffolds was measured in PBS solution using UV spectrophotometry at 37 °C. Fig. 8 shows the release profiles of scaffolds with different ENR-loaded contents from 0.2 wt% to 1.4 wt%. As observed, all of the ENR release profiles presented the similar behavior in the release research period, consisting of an initial burst release in the first 20 h and a secondary sustained release after that. To be specific, the accumulate release percentages of ENR from ENR-loaded scaffolds 0.2 wt% ENR, 0.8 wt% ENR, and 1.4 wt% ENR in the first 20 h were 65%, 73% and 80%, respectively. Moreover, the accumulate release percentages of ENR from ENR-loaded scaffolds containing 0.2 wt%, 0.8 wt% and 1.4 wt% ENR within 185 h were 88%, 94% and 96%, respectively. Obviously, the release rate of ENR gradually increased with the increase of drug loading amount of ENR. This should be because the more ENR loaded on the porous scaffolds, the higher concentration difference of ENR between the matrix of the scaffold and release solution.

Antibacterial activity of porous scaffolds

The antibacterial activity of the porous scaffolds against *S. aureus* and *E. coli* were assessed *via* the inhibition zone method. The relevant experimental results are shown in Fig. 9. Obviously, the control porous scaffolds without ENR displayed no observable inhibition zones, indicating that the control porous scaffolds had no antibacterial activity against *S. aureus* and *E. coli*. However, the ENR loaded porous scaffolds generated apparently inhibition zones, which suggested that the ENR loaded porous scaffolds performed outstanding antibacterial activity against *S. aureus* and *E. coli.* Besides, it was seen from Fig. $9a_1$–a_3 that the inhibition zones of 1.4% ENR loaded porous scaffolds were no observable reduction after 120 h incubation, which displayed that the ENR loaded porous scaffolds possessed the long-term antimicrobial effect against *S. aureus* and *E. coli*. Moreover, after 24 h incubation, it was found from Fig. $9b_1$ that the inhibition zone of 1.4% ENR loaded porous

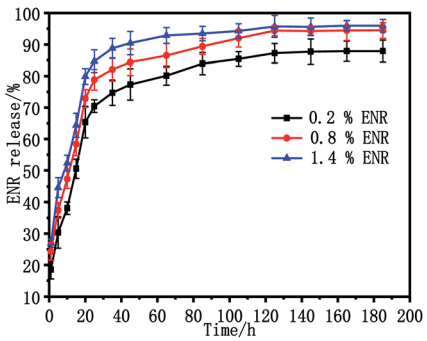

Fig. 8 *In vitro* release profiles of ENR from ENR-loaded porous scaffolds in PBS solution at 37 °C.

scaffolds was clearly larger than those of 0.2% and 0.8% ENR loaded porous scaffolds. This was probably because the ENR loaded amount and related cumulative release ratio of 1.4% ENR loaded porous scaffolds were higher than those of 0.2% and 0.8% ENR loaded porous scaffolds. Basing on the above results, the ENR loaded porous scaffolds displayed the long-term and outstanding antibacterial activity against *S. aureus* and *E. coli*, and the antibacterial activity could be adjusted by changing the drug loaded amount.

In vitro biocompatibility assessment

In vitro mBMSCs cell culture experiment was used to evaluate the biocompatibility of the porous scaffolds samples. In this research, the morphology of mBMSCs seeded on porous scaffolds was characterized with an inverted fluorescent microscope (IX53, Olympus). Fig. 10a–c show the mBMSCs cultured on the porous scaffolds samples without adding Ms-PCL as control samples of live/dead staining assay after culturing for 72 h. The relative culture results of porous scaffolds samples with adding Ms-PCL could be observed in Fig. 10d–f. As observed, a large amount of mBMSCs presenting a spindle shape had proliferated on the porous scaffolds samples without a large number of dead cells, which proved that the mBMSCs could adhere to the porous scaffolds well. Furthermore, the result of cell multiplication on porous scaffolds was evaluated by Spectra Max fluorescence microplate reader (Molecular Devices) and showed in Fig. 10g. After cultured for 1, 3, 5 days, the number of mBMSCs on the porous scaffolds samples had a significant increase, indicating the excellent adhesion and proliferation of mBMSCs on porous scaffolds samples. Compared with the control samples, the number of cells proliferated in the porous scaffolds samples containing Ms-PCL was greater. The main reason may be the surface of the samples became rougher after adding Ms-PCL, which was conducive to cells adhesion and proliferation.

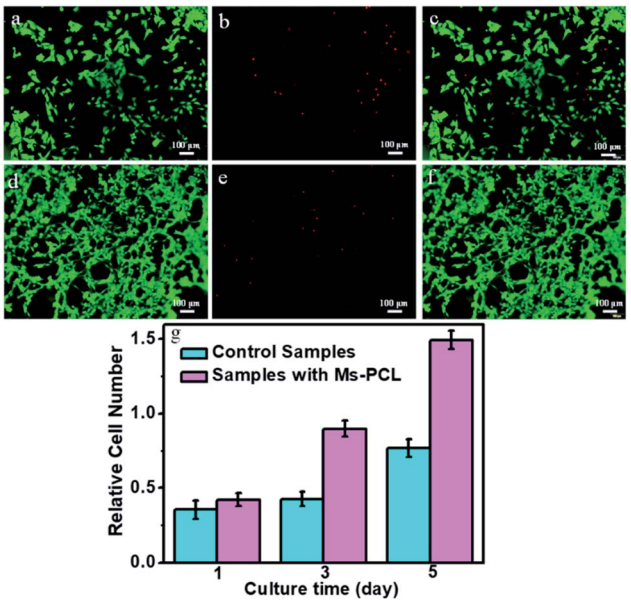

Fig. 10 The fluorescence microscopy of mBMSCs morphology after culture for 72 h in culture medium of control samples without Ms-PCL ((a) live, (b) dead, (c) merged) and the samples containing Ms-PCL ((d) live, (e) dead, (f) merged), and (g) proliferation rate of mBMSCs after cultivating 1, 3, 5 days on porous scaffolds samples.

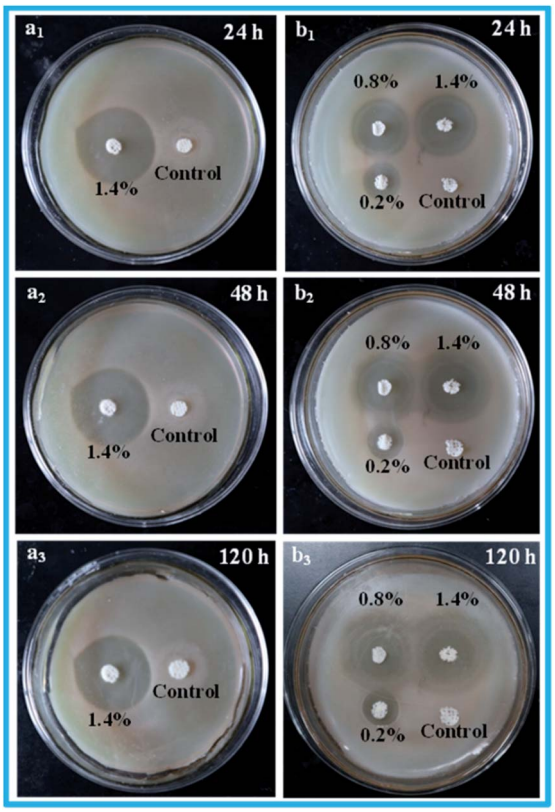

Fig. 9 Antibacterial activities of 1.4% ENR loaded porous scaffolds with different storage times against *S. aureus*: (a_1) 24 h, (a_2) 48 h, (a_3) 120 h; and the antibacterial activities of 0.2%, 0.8%, 1.4% ENR loaded porous scaffolds with different storage times against *E. coli*: (b_1) 24 h, (b_2) 48 h, (b_3) 120 h.

Conclusions

In this work, the biocompatible SA/Col porous scaffolds containing Ms-PCL had been facilely fabricated based on 3D extrusion printing of the pre-crosslinked SA/Col hydrogels. GP had been chosen as a biocompatible cross-linking agent for Col, and SA network had been introduced into pure Col hydrogels in order to construct the double networks, which had significantly improved the mechanical properties and reduced the degradation rate of composite SA/Col hydrogels. Moreover, the Ms-PCL prepared by solvent evaporation were added to the SA/Col hydrogels, and the *in vitro* drug release experiments showed that the composite hydrogels had a sustained drug release function. In addition, the antibacterial experiments showed that the composite SA/Col scaffolds displayed a distinguished and long-term antibacterial activity against *E. coli* and *S. aureus*. Besides, the *in vitro* biocompatibility experiments displayed that the mBMSCs could be adhered well on the composite scaffolds, which indicated that the fabricated composite SA/Col

scaffolds were biocompatible. In short, the strategy for fabricating the composite SA/Col scaffolds represents a new method to the use of biocompatible injectable and 3D printable hydrogels for cartilage regeneration in bone tissue engineering.

Conflicts of interest

There are no conflicts of interest to declare.

Acknowledgements

The financial support by International Science and Technology Cooperation Project of Guangzhou Economic Technological Development Zone (2017GH09), the National Natural Science Foundation of China (51703067), Natural Science Foundation of Guangdong Province (2020A1515011004, 2020A0505100050, 2020A151501823), Special research project in Guangdong Universities. 2019 Innovation Team Project of Shaoguang City, High Class Scientific Technology Project of SCAU (4900-219390) are gratefully acknowledged.

Notes and references

1 Y. B. Zhang, J. K. Yu, K. X. Ren, J. L. Zuo, J. X. Ding and X. S. Chen, *Biomacromolecules*, 2019, **20**, 1478.
2 W. Kim and G. Kim, *Biofabrication*, 2020, **12**(1), 015007.
3 H. S. Du, W. M. Liu, M. L. Zhang, C. L. Si, X. Y. Zhang and B. Li, *Carbohydr. Polym.*, 2019, **209**, 130.
4 D. Lin, Y. J. Chai, Y. F. Ma, B. Duan, Y. Yuan and C. S. Liu, *Biomaterials*, 2019, **196**, 122.
5 H. Amani, E. Mostafavi, H. Arzaghi, S. Davaran, A. Akbarzadeh, O. Akhavan, H. Pazoki-Toroudi and T. J. Webster, *ACS Biomater. Sci. Eng.*, 2019, **5**, 193.
6 J. Chen, T. H. Zhang, W. K. Hua, P. Y. Li and X. F. Wang, *Colloids Surf., A*, 2020, **585**, 124048.
7 L. Roseti, V. Parisi, M. Petretta, C. Cavallo, G. Desando, I. Bartolotti and B. Grigolo, *Mater. Sci. Eng., C*, 2017, **78**, 1246.
8 Y. N. Jiang, J. P. Zhou, H. C. Shi, G. Q. Zhao, Q. Zhang, C. Feng and X. D. Xv, *J. Mater. Sci.*, 2020, **55**, 2618.
9 S. Kajave Nilabh, T. Schmitt, N. Thuy-Uyen and K. Vipuil, *Mater. Sci. Eng., C*, 2020, **107**, 110290.
10 S. R. Radhika Rajasree, M. Gobalakrishnan, L. Aranganathan and M. G. Karthih, *Mater. Sci. Eng., C*, 2020, **107**, 110270.
11 K. K. Moncal, R. S. T. Aydin, M. Abu-Laban, D. N. Heo, E. Rizk, S. M. Tucker, G. S. Lewis, D. Hayes and I. T. Ozbolat, *Mater. Sci. Eng., C*, 2019, **105**, 110128.
12 H. Wu, Y. Song, J. Q. Li, X. Lei, S. S. Zhang, Y. Gao, P. Z. Cheng, B. Liu, S. Miao, L. Bi, L. Yang and G. X. Pei, *Cell Proliferation*, 2019, 12725.
13 K. N. Bardakova, E. A. Grebenik, N. V. Minaev, S. N. Churbanov, Z. Moldagazyeva, G. E. Krupinov, S. V. Kostjuk and P. S. Timashev, *Mater. Sci. Eng., C*, 2020, **107**, 110300.
14 S. Sayed, O. Faruq, M. Hossain, S. B. Im, Y. S. Kim and B. T. Lee, *Mater. Sci. Eng., C*, 2019, **105**, 110027.
15 Y. N. Liu and D. D. Fan, *Int. J. Biol. Macromol.*, 2019, **141**, 700.
16 S. Lohrasbi, E. Mirzaei, A. Karimizade, S. Takallu and A. Rezaei, *Cellulose*, 2020, **27**, 927–940.
17 M. H. Nabavi, M. Salehi, A. Ehterami, F. Bastami, H. Semyari, M. Tehranchi, M. A. Nabavi and H. Semyari, *Drug Deliv. Transl. Res.*, 2019, **10**, 108.
18 Y. Nakamuta, T. Arahira and M. Todo, *J. Mater. Sci.: Mater. Med.*, 2019, **30**, 119.
19 D. N. Heo, M. Hospodiuk and I. T. Ozbolat, *Acta Biomater.*, 2019, **95**, 348.
20 P. Pal, Q. C. Nguyen, A. H. Benton, M. E. Marquart and A. V. Janorkar, *Macromol. Biosci.*, 2019, **19**, 1900142.
21 Y. P. Lee, H. Y. Liu, P. C. Lin, Y. H. Lee, L. R. Yu, C. C. Hsieh, P. J. Shih, W. P. Shih, I. J. Wang, J. Y. Yen and C. A. Dai, *Colloids Surf., B*, 2019, **175**, 26.
22 K. Q. Huang, J. Wu and Z. P. Gu, *ACS Appl. Mater. Interfaces*, 2019, **11**, 2908.
23 A. Oryan, A. Kamali, A. Moshiri, H. Baharvand and H. Daemi, *Int. J. Biol. Macromol.*, 2018, **107**, 678.
24 N. Reddy, R. Reddy and Q. R. Jiang, *Trends Biotechnol.*, 2015, **33**, 6.
25 K. L. Spiller, R. R. Anfang, K. J. Spiller, J. Ng, K. R. Nakazawa, J. W. Daulton and G. Vunjak-Noyakovic, *Biomaterials*, 2014, **35**(15), 4477.
26 A. O. Elzoghby, W. S. A. El-Fotoh and N. A. Elgindy, *J. Controlled Release*, 2011, **153**, 206.
27 S. M. Lien, L. Y. Ko and T. J. Huang, *Acta Biomater.*, 2009, **5**, 670.
28 X. Luo, B. Lin, Y. G. Gao, X. H. Lei, X. Wang, Y. F. Li and T. Li, *Int. Immunopharmacol.*, 2019, **76**, 105842.
29 V. Perez-Puyana, M. Jimenez-Rosado, A. Romero and A. Guerrero, *Int. J. Biol. Macromol.*, 2019, **139**, 262.
30 J. Lewandowska-Lancucka, A. Gilarska, A. Bula, W. Horak, A. Latkiewicz and M. Nowakowska, *Int. J. Biol. Macromol.*, 2019, **136**, 1196.
31 Z. H. Lu, S. J. Liu, Y. G. Le, Z. N. Qin, M. W. He, F. B. Xu, Y. Zhu, J. M. Zhao, C. B. Mao and L. Zheng, *Biomaterials*, 2019, **218**, 119190.
32 Y. Koo, E. J. Choi, J. Lee, H. J. Kim, G. Kim and S. H. Do, *J. Ind. Eng. Chem.*, 2018, **66**, 34.
33 O. Akturk, K. Kismet, A. C. Yasti, S. Kuru, M. E. Duymus, F. Kaya, M. Caydere, S. Hucumenoglu and D. Keskin, *J. Biomater. Appl.*, 2016, **31**(2), 283.
34 K. H. Kwan, X. Liu, M. K. To, K. W. Yeung, C. M. Ho and K. K. Wong, *Nanomedicine*, 2011, **7**(4), 497.
35 R. Xing, K. Liu, T. Jiao, N. Zhang, K. Ma, R. Zhang, Q. Zou, G. Ma and X. Yan, *Adv. Mater.*, 2016, **28**(19), 3669.
36 M. Shkir, I. S. Yahia, M. Kilany, M. M. Abutalib, S. AlFaify and R. Darwish, *Ceram. Int.*, 2019, **45**, 50.
37 M. Farokhi, F. Mottaghitalab, S. Samani, M. A. Shokrgozar, S. C. Kundu, R. L. Reis and Y. Fatahi, *Biotechnol. Adv.*, 2018, **36**, 68.
38 H. Zhou and J. Lee, *Acta Biomater.*, 2011, **7**, 2769.
39 O. Jeon, K. H. Bouhadir, J. M. Mansour and E. Alsberg, *Biomaterials*, 2009, **30**, 2724.
40 S. M. Hong, D. Sycks, H. F. Chan, S. T. Lin, G. P. Lopez, F. Guilak, K. W. Leong and X. H. Zhao, *Adv. Mater.*, 2015, **27**, 4035.

41 M. Z. Moghadam, S. Hassanajili, F. Esmaeilzadeh, M. Ayatollahi and M. Ahmadi, *J. Mech. Behav. Biomed. Mater.*, 2017, **69**, 115.
42 S. A. Poursamar, A. N. Lehner, M. Azami, S. Ebrahimi-Barough, A. Samadikuchaksaraei and A. P. M. Antunes, *Mater. Sci. Eng., C*, 2016, **63**, 1.
43 Y. Hu, J. G. Wang, X. Li, X. X. Hu, W. Y. Zhou, X. M. Dong, C. Y. Wang, Z. H. Yang and B. P. Binks, *J. Colloid Interface Sci.*, 2019, **545**, 104.
44 Y. Hu, S. S. Ma, Z. H. Yang, W. Y. Zhou, Z. S. Du, J. Huang, H. Yi and C. Y. Wang, *Colloids Surf., B*, 2016, **140**, 382.
45 B. P. Binks, *Adv. Mater.*, 2002, **14**, 1824.
46 Y. F. Jin, C. C. Liu, W. X. Chai, A. Compaan and Y. Huang, *ACS Appl. Mater. Interfaces*, 2017, **9**, 17456.
47 Y. F. Jin, A. Compaan, W. X. Chai and Y. Huang, *ACS Appl. Mater. Interfaces*, 2017, **9**, 20057.
48 S. Vijayavenkataraman, W. C. Yan, W. F. Lu, C. H. Wang and J. Y. H. Fuh, *Adv. Drug Delivery Rev.*, 2018, **132**, 296.
49 K. Vithani, A. Goyanes, V. Jannin, A. W. Basit, S. Gaisford and B. J. Boyd, *Pharm. Res.*, 2019, **36**, 4.
50 Y. Kang, C. L. Wang, Y. B. Qiao, J. W. Gu, H. Zhang, T. Peijs, J. Kong, G. C. Zhang and X. T. Shi, *Biomacromolecules*, 2019, **20**, 1765.
51 L. Chen, C. J. Deng, J. Y. Li, Q. Q. Yao, J. Chang, L. M. Wang and C. T. Wu, *Biomaterials*, 2019, **196**, 138.
52 W. T. Jia, P. S. Gungor-Ozkerim, Y. S. Zhang, K. Yue, K. Zhu, W. J. Liu, Q. Pi, B. Byambaa, M. R. Dokmeci, S. R. Shin and A. Khademhosseini, *Biomaterials*, 2016, **106**, 58.
53 S. F. Liu, Y. Hu, J. C. Zhang, S. Q. Bao, L. Xian, X. M. Dong, W. X. Zheng, Y. H. Li, H. C. Gao and W. Y. Zhou, *Macromol. Mater. Eng.*, 2019, **304**, 1800698.
54 G. G. F. Nascimento, J. Locatelli, P. C. Freitas and G. L. Silva, *Braz. J. Microbiol.*, 2000, **31**(4), 247.
55 W. Brostow, S. Brumbley, M. Gahutishvili and N. Hnatchuk, *Macromol. Symp.*, 2016, **365**, 258.
56 M. F. Butler, Y. F. Ng and P. D. A. Pudney, *J. Polym. Sci., Part A: Polym. Chem.*, 2003, **41**(24), 3941.
57 R. A. A. Muzzarelli, *Carbohydr. Polym.*, 2009, **77**, 1.
58 Z. H. Wei, Y. J. Cheng, J. Y. Zhu and Q. R. Huang, *Food Hydrocolloids*, 2019, **94**, 561.
59 Z. H. Lu, S. J. Liu, Y. G. Le, Z. N. Qin, M. W. He, F. B. Xu, Y. Zhu, J. M. Zhao, C. B. Mao and L. Zheng, *Biomaterials*, 2019, **218**, 119190.